
The Theory of Compensated Laser Propagation through Strong Thermal Blooming

Jonathan F. Schonfeld

■ Thermal blooming is the spreading of a laser beam that results when some of the beam's energy is absorbed by the medium that the beam is propagating through. If left uncorrected, the spreading would significantly reduce the effectiveness of high-power lasers as directed-energy weapons and as devices for beaming power over long paths through the atmosphere. In this article we survey the theory of adaptive compensation for thermal blooming, with an emphasis on research at Lincoln Laboratory since 1985. This work includes the development of MOLLY, a uniquely realistic computer simulation of adaptively compensated laser propagation through turbulence and thermal blooming, and the development of robust experimental signatures for important fundamental processes, most notably phase-compensation instability (PCI). Caused by positive feedback between an adaptive optics system and laser-induced atmospheric heating, PCI can strain the capabilities of adaptive optics hardware. Results from both MOLLY, which was optimized for the Cray-2 supercomputer, and our analysis of PCI have been verified in laboratory and field experiments.

In this article, we discuss the physics of uncompensated and compensated thermal blooming, the architecture and capabilities of MOLLY, and an analysis of PCI that takes into account the detailed structure of adaptive optics hardware. Finally, we use MOLLY output to illustrate signatures of PCI, effects that ameliorate PCI, and characteristic trends that make it possible to predict large-system performance from subscale experiments.

THEMICAL BLOOMING OCCURS when a laser beam spreads in response to its own heating of the medium through which it propagates. Compensation for thermal blooming will be required if a high-power laser is used, for example, as a directed-energy weapon, as in the Strategic Defense Initiative (SDI) concept of ground-based-laser ballistic-missile defense. Compensation for thermal blooming is also required when a high-power laser is used to deliver large amounts of useful power over long distances through the atmosphere to reduce onboard-power requirements for earth-orbiting satellites, for exam-

ple, or to transmit power directly to a lunar station.

Compensation for thermal blooming relies on the same principles of adaptive optics used in atmospheric-turbulence compensation [1, 2]. In the compensation process, a phase sensor measures the reference wavefront of a beacon coming from above the atmosphere, and a deformable mirror applies in real time the inverse of the sensed aberrations (i.e., the conjugate phase) to the outgoing (high-power) laser beam to compensate the beam's wavefront for the aberrations. The phase of the laser beam at the top of the atmosphere is thereby made nearly diffraction lim-

ited. Turbulence and thermal blooming can, of course, occur together, and a wavefront sensor cannot decompose an aberration on an incoming wavefront into two separate components, one due to turbulence and the other to thermal blooming.

When thermal blooming is present, compensation with adaptive optics is complicated by several factors that are not present when lasers of relatively low power are used, i.e., when only turbulence matters. Most importantly, thermal blooming creates feedback between the adaptive optics and the propagation medium: a transmitted laser wavefront is modified by the adaptive optics system, which leads to a change in the irradiance pattern of the propagating beam, which in turn causes a perturbation in the beam-induced atmospheric heating that the adaptive optics system was initially trying to correct. This feedback results in phase-compensation instability (PCI), which, under extreme conditions, can lead laser-induced atmospheric heating to form patterns of irradiance and phase distributions that cannot be corrected by the adaptive optics hardware.

In this article, we survey contributions by Lincoln Laboratory to the theory of adaptive compensation for thermal blooming with a special emphasis on developments since 1985, when SDI objectives focused attention on very large laser systems with stronger thermal blooming than was previously contemplated. This period also saw the emergence of PCI as a dominant technical concern, which led to the first use of high-performance supercomputers for thermal-blooming modeling. Lincoln Laboratory is one of a number of organizations that have significantly contributed to the theory of adaptive compensation for thermal blooming [3].

Before beginning our survey, we introduce the basic physics of thermal blooming and PCI. We then articulate the broad framework of the Lincoln Laboratory program in thermal-blooming theory and highlight a cornerstone of this program: MOLLY, a supercomputer model that has come to define the state of the art in the numerical simulation of adaptively compensated laser propagation through turbulence and thermal blooming. Finally, we use MOLLY output to illustrate the basic phenomena of thermal-blooming compensation and particular fea-

tures of thermal-blooming compensation in very large systems.

Physics of Thermal Blooming

The basic properties of thermal blooming are governed by the absorption of laser energy and by the flow of the medium that the laser beam is propagating through. The absorption determines the amount of heat available for perturbing the index of refraction in the propagation medium, and the flow determines the time available for the heated medium to affect laser propagation before it is swept out of the beam.

In quantitative terms, let I represent the laser irradiance, i.e., the power propagated by a laser across a unit area perpendicular to the direction of propagation. The power absorbed by the medium per unit volume is then αI , where α is the absorption per unit length, or absorptivity. This absorption produces a temperature change per unit time of $\alpha I / \rho c_p$, where ρ is the mass density of the medium and c_p is the specific heat at constant pressure. This temperature change per unit time in turn produces an index-of-refraction change per unit time of

$$\left(\frac{\alpha I}{\rho c_p} \right) \frac{dn}{dT},$$

where n is the refractivity and T is the temperature. These estimates assume that the absorbed energy is transformed instantaneously into heat, and that the heat instantaneously results in a change in the index of refraction of the propagation medium. Both assumptions are appropriate for this article. Typically, refractivity decreases (toward unity, its value *in vacuo*) with increasing temperature. Thus dn/dT is negative, so the laser beam transforms the medium through which it propagates into a diverging lens, directly leading the beam to spread, or bloom—hence the term thermal blooming.

The strength of this lens is limited by the transport of heated air out of the beam's path in a time of order D/v , where D is the beam's diameter and v is the relative speed between the beam and the propagation medium in a direction transverse to the beam direction. The variable v receives contributions from ma-

terial flow as well as from slew, which is defined as the angular motion of a beam when tracking a moving target. The quantity $\tau = D/v$, known as the wind-clearing time, represents a fundamental relaxation time for transient phenomena in thermal blooming. The total change in the index of refraction induced by a laser beam in an absorbing medium is thus

$$\text{O}\left(\frac{\alpha I}{\rho c_p} \left(\frac{dn}{dT}\right) \frac{D}{v}\right),$$

associated with a total change

$$\text{O}\left(\left(\frac{\alpha I}{\rho c_p}\right) \frac{D}{v}\right)$$

in the temperature of the propagation medium.

This laser-induced change in refractivity in turn induces an aberration

$$\text{O}\left(\frac{\alpha I}{\rho c_p} \left(\frac{dn}{dT}\right) \frac{D}{v} kL\right) \quad (1)$$

in the laser beam's phase, where k is the laser wave number (equal to 2π divided by the laser wavelength) and L is the length of the absorbing portion of the propagation medium.

For a feel for the size of these effects, consider the unslewed vertical propagation—from ground to space through desert air flowing at a wind speed of 3 m/sec (a relatively calm day)—of a 1.06-μm high-power laser with an irradiance of 1 MW/m² and a beam diameter of 3.5 m. At this wavelength, which lies in an atmospheric transmission window [4] where the absorptivity is dominated by aerosol particles [5], $\alpha \approx 0.002 \text{ km}^{-1}$ and $L \approx 2 \text{ km}$ [6]. Combining these numbers with

$$\frac{1}{\rho c_p} \approx 770 \text{ cc}^\circ\text{C / J},$$

$$\frac{1}{\rho c_p} \frac{dn}{dT} \approx -7.7 \times 10^{-4} \text{ cc / J}$$

at 27°C, we obtain a laser-induced refractivity perturbation of roughly 2×10^{-9} associated with a temperature rise of $\sim 0.002^\circ\text{C}$. This perturbation will

produce an integrated phase aberration of roughly 20 radians. The $\sim 0.002^\circ$ temperature rise is much smaller than the $O(0.1^\circ\text{C})$ that is typical of the temperature fluctuations associated with atmospheric turbulence. The temperature fluctuations due to thermal blooming, however, are much more effective in producing phase aberrations than fluctuations due to turbulence because the blooming fluctuations all have the same sign, and they thus add constructively.

The conventional measure of the optical strength of thermal blooming is given by the distortion number N_D . First introduced by Lee C. Bradley III and Jan Herrmann of Lincoln Laboratory in 1974 [7], N_D is defined by

$$N_D \equiv \int_0^{\infty} \left(\frac{4\sqrt{2kP}}{\rho c_p D} \right) \frac{dn}{dT} \frac{\alpha(z)}{v(z)} e^{-\int_0^z [\alpha(z') + \alpha_s(z')] dz'} dz,$$

where z is the propagation distance, P is the laser power, and α_s is the scattering coefficient. This equation generalizes Expression 1 (if one identifies I with P/D^2) to scenarios in which absorption and wind (including slew) vary with propagation distance, and in which attenuation of the laser beam is sizable. As a rule of thumb, the total peak-to-valley phase aberration in radians is approximately $N_D/3$ for a laser beam with a Gaussian irradiance profile.

Figure 1 illustrates the spreading of far-field irradiance due to thermal blooming with $N_D = 50$. The characteristic asymmetry seen in the figure is caused by the wind. To understand this phenomenon, consider the distribution of laser-induced heating in the absorbing medium. Points in the medium at both the upwind and downwind edges of the beam are heated by the beam, but the downwind points are also heated by the wind-driven transport of hot medium from the upwind edge. Thus the laser-induced change in index of refraction is more negative downwind than upwind, and consequently the laser-induced phase aberrations tilt the beam into the wind. The result is the crescent seen in Figure 1.

Figure 2 schematically illustrates the characteristic dependence of peak far-field irradiance I_{peak} on transmitted laser power P in the presence of thermal blooming. Without absorption, the curve of I_{peak} versus P would be a straight line. In the presence of thermal

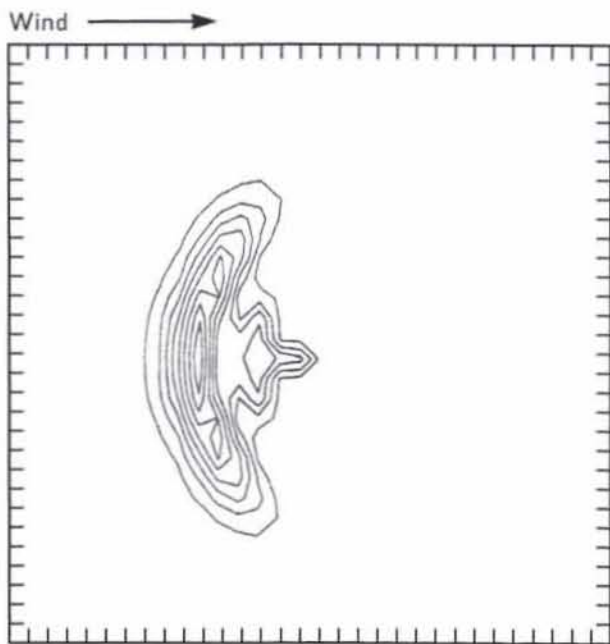


FIGURE 1. Far-field irradiance pattern of a thermally bloomed beam with thermal-blooming distortion number $N_D = 50$. The spacing between tick marks in the figure is two-thirds the diameter of an unaberrated (diffraction-limited) spot. The contour spacing is one-ninth the peak irradiance.

blooming, the curve exhibits a maximum, at which point further increases in power result in decreasing irradiance. The power at the point of diminishing returns is referred to as the critical power P_{crit} . Adaptive optics can increase both the value of P_{crit} and the value of the corresponding irradiance I_{crit} , but even with adaptive optics we expect that the I_{peak} -versus- P curve will exhibit a maximum irradiance, at which

point a further increase in power will not result in a further increase in irradiance.

Atmospheric turbulence can exacerbate the effects of thermal blooming. Turbulence causes a propagating laser beam to become scintillated; i.e., the beam develops irradiance variation on small scales transverse to the propagation direction. Thus turbulence can cause the heating that is deposited by the laser beam to vary on small transverse scales, producing strong phase gradients that directly increase the angular spreading of the far-field irradiance pattern. The effectiveness of the adaptive optics can be undercut when the scale of the spatial variation that the turbulence-induced scintillation imposes on a thermal-blooming phase aberration is smaller than the smallest scale resolvable by the deformable mirror used in the adaptive optics system. This interplay between turbulence and thermal blooming, known as turbulence/thermal-blooming interaction (TTBI), was first described by Herrmann of Lincoln Laboratory in the early 1980s [8]. TTBI became a major focus of study in the late 1980s [3].

Phase-Compensation Instability (PCI)

As explained earlier, a phase-conjugate adaptive optics system can compensate for thermal-blooming phase aberrations just as it can for turbulence. At very strong levels of blooming, however, the adaptive optics system itself can provoke the growth of a strong variation in phase aberrations on small scales transverse to the propagation direction. This phenomenon, referred to as phase-compensation instability

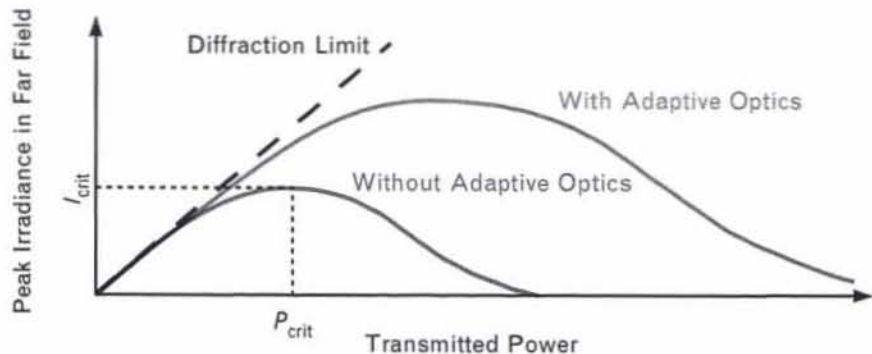


FIGURE 2. Schematic behavior of the peak irradiance in the far field of a laser beam subjected to thermal blooming. The line labeled "Diffraction Limit" refers to unaberrated propagation.

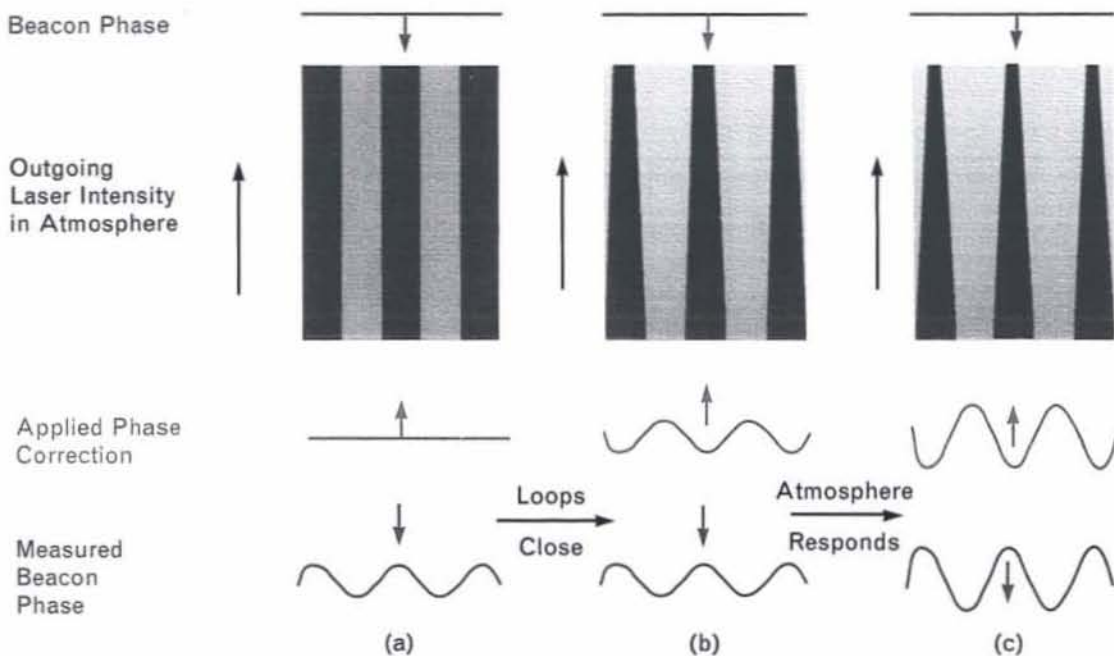


FIGURE 3. Phase-compensation instability (PCI) mechanism: (a) Strong and weak spots that occur naturally in the outgoing laser irradiance induce hot and cold regions (denoted by dark and light areas, respectively) in the atmosphere. A wavefront sensor detects valleys and peaks in the aberrated wavefront of a beacon due to the beacon's passage through atmospheric regions that are relatively hot and cold, respectively. (b) A deformable mirror compensates the aberration by applying to the outgoing beam a phase that has peaks beneath hot regions and valleys beneath cool ones. (Note: The deformable-mirror surface will have valleys and peaks where the applied phase has peaks and valleys, respectively.) Thus the deformable mirror has the effect of focusing the outgoing beam into hot regions, making them hotter. Again, the hot and cold regions distort the measured beacon phase, and (c) the distortion causes the deformable mirror to focus even harder into the hot regions.

(PCI), is illustrated in Figure 3. The figure shows schematically the evolution in time of a set of hot and cold regions in the propagation medium. Denoted by dark and light areas, respectively, the hot and cold regions can be induced initially by strong and weak spots occurring naturally in the outgoing laser irradiance. The hot and cold regions distort the measured phase of the beacon. In its attempts to compensate the aberrated beacon phase, the correction system focuses the outgoing laser beam into the atmospheric hot spots, making them hotter, which, in turn, results in an even greater aberration of the measured beacon phase.

The possibility of positive feedback between adaptive optics and thermal blooming was first raised by Herrmann of Lincoln Laboratory in 1977 [9], and explored with a mathematical model that idealizes the

absorbing medium as a simple lens whose strength depends on the irradiance of the laser beam propagating through it. Subsequently, the growth of small-scale structures was observed in steady-state computer simulations of compensated strong thermal blooming. Although this result was tentatively identified as a physical instability, researchers suspected at the time that computational artifacts might be playing a role [10]. The modern period in the theory of PCI was initiated in 1986 through 1987 by the introduction of linearized PCI analyses [11–14] that were not linked to a simple-lens idealization, and by the advent of fully time-dependent simulations of thermal blooming with supercomputers.

As it turns out, the rate at which PCI develops increases roughly as the spatial scale that the adaptive optics system can resolve decreases [14]. In practice,

this scale is calibrated in terms of the perturbation Fresnel number $N_p = \pi n a^2 / \lambda L$, where n and L are the refractivity and depth, respectively, of the absorbing medium, a is the actuator spacing of the adaptive optics system, and λ is the laser wavelength. One might imagine inhibiting PCI by using a coarse actuator spacing. This strategy is often not practical, however, in situations where turbulence and thermal blooming are present at the same time—turbulence, which can cause aberrations that have high spatial frequencies, cannot be corrected effectively when the actuator spacing is too coarse.

Several factors reduce the practical impact of PCI. First, wind clearing limits the growth of PCI because a beam-induced change in the propagation medium can affect subsequent propagation only as long as the heated material remains in the beam. Second, wind variation (including the contribution of slew) along the propagation direction also inhibits PCI. When the magnitude or direction of the wind takes different values at different distances from the laser transmitter, the atmosphere cannot sustain patterns of hot and cold that line up with the propagation direction as they do in Figure 3. Wind variations thus offset the tendency for contributions to PCI from different distances along the beam to reinforce one another. Finally, PCI is damped by thermal diffusion and turbulent diffusion, which tend to wash out thermal inhomogeneities. This effect is relatively unimportant in the open air, but thermal diffusion can be significant in a laboratory thermal-blooming experiment with a small beam propagating through an absorbing liquid [15].

Thermal-Blooming Theory at Lincoln Laboratory

Work on the theory of thermal blooming began at Lincoln Laboratory in the late 1960s, when Bradley and Herrmann developed a steady-state computer simulation of laser propagation through an absorbing medium [16]. The simulation was the first to represent uncompensated thermal blooming accurately. From a mathematical standpoint, the simulation was notable for implementing numerical techniques that avoided spurious sources or sinks of laser energy, and for employing a coordinate system whose resolution

transverse to the propagation direction varied with propagation distance. The coordinate system permitted the accurate representation of the beam even when the beam spread under the influence of strong thermal blooming and when it became small because of focusing. Numerical simulation has figured prominently in thermal-blooming theory at Lincoln Laboratory ever since.

The steady-state propagation code was in continuous use and development until the mid-1980s. At that time, SDI ground-based ballistic-missile-defense mission requirements—laser apertures several meters in diameter and distortion numbers of several hundred or more—highlighted a number of simulation limitations that further incremental changes in the steady-state code could not overcome. One of the limitations was that the steady state was computed as the result of a mathematical iteration that bore no direct relation to the physical passage of time. Thus, when indications of instability at a high distortion number were first observed, it was difficult to decide whether to ascribe them to a real physical effect, to a breakdown in convergence due to a numerical difficulty, or simply to the nonexistence of a true steady state. Another limitation of the code was that there can in fact be no steady state for thermal blooming in the presence of turbulence because wind-blown turbulence is inherently time dependent. Finally, because the steady-state code was not optimized for vector computer architectures, it could not exploit the speed and large memory of modern supercomputers. This last point was especially important because the prospect of simulating processes (e.g., PCI) that create significant structure on small scales over long propagation paths pointed to a need for fine spatial resolution, which requires the storage and processing of very large amounts of data.

Accordingly, in 1986 I undertook the development of a new computer simulation of the time-dependent behavior of adaptively compensated laser propagation through turbulence and strong thermal blooming [17]. The new computer code, named MOLLY after the character Molly Bloom in James Joyce's Ulysses [18], was optimized for operation on the Cray-2 supercomputer, notable for its speed (400 Mflops peak on each of four processors) and memory (256

Mwords). In addition, the Cray-2's long word size of 64 bits provided additional insurance against numerical artifacts that were not provided for by the 32-bit computers for which the steady-state code was designed. The Cray-2's large memory has permitted us to use MOLLY to simulate with impunity scenarios that other organizations have been unable to simulate at all.

MOLLY has come to define the state of the art in the numerical simulation of adaptively compensated high-power-laser propagation. The code is noteworthy for the realism with which it models adaptive optics hardware, and for a number of structural innovations that have made it uniquely flexible and efficient. MOLLY's design will be discussed in greater detail in the following section.

The fundamental questions stressed in the application and continuing development of MOLLY have been the following:

1. Is PCI a real phenomenon?
2. What physical processes ameliorate it?
3. What is its impact on the effectiveness of systems that use high-power lasers?

We have learned much of what we know about the answers to these questions, especially the third, through the exploratory application of MOLLY. The code has also been used extensively to plan and interpret experiments, and it has in turn been verified by comparison with the results of those experiments [15, 19].

In addition to code development, we have pursued the development of the analytical theory of PCI. Only a few years ago, the analytical theory (as Reference 14 exemplifies) was not sufficiently advanced to provide decisive signatures of PCI for high-distortion-number experiments and simulations. In particular, the theory assumed closeness to certain idealized conditions that, if the propagating beam was sufficiently powerful, could remain valid only for a short time. Moreover, the early theory was developed for a simplified model of the adaptive optics hardware. For example, the model did not take into account that real wavefront-sensor subapertures and deformable-mirror actuators are arranged on fixed (usually square), finite-resolution grids. The development of analytical theory at Lincoln Laboratory has kept pace with computer modeling over the past five years: the develop-

ment has focused on the generalization of the analytical theory of PCI for adaptive optics models with a realistic grid geometry, and on the search for analytical predictions that transcend small-time limitations [20]. This development will be discussed further in the section "Simulation Results."

The MOLLY Code

MOLLY simulates the time evolution of a laser field, the laser- and turbulence-induced refractivity variations, and the adaptive optics components, all on rectangular grids perpendicular to the propagation direction. Time is discretized by idealizing the laser beam as a sequence of instantaneous pulses. MOLLY places no restrictions on the order in which high-power-laser pulses, beacon-laser pulses, and intervals of medium transport occur, nor on the relations between parameters (such as wavelengths and absorptivities) that govern the dynamics of distinct laser pulses. This scheduling flexibility enables MOLLY to simulate easily and efficiently the thermal blooming produced, for example, by a multiline chemical laser (such as the Alpha Verification Module used in the SABLE experiment described in Reference 19). For the purpose of simulation, such a laser must be treated as an ensemble of lasers, one for each spectral line. MOLLY's scheduling flexibility also facilitates simulations of scenarios that use a synthetic beacon (an adaptive optics beacon source produced by the backscatter of a laser beam focused high in the atmosphere [21]). In such cases, MOLLY must choreograph the propagation of an outgoing high-power laser, an incoming tracking beam, an outgoing synthetic-beacon laser beam, and a statistical ensemble of return propagations that represents the incoherent backscatter from the synthetic beacon.

To keep MOLLY running fast, we held the code to the following standard: with very few exceptions, all algorithms involving any of the aforementioned grids require at most $O(N \log^2 N)$ arithmetic operations, where N is the number of points in the grid in question. In large part, this restriction was accomplished through the liberal use of fast Fourier transforms, which not only promoted speed but, as we shall see, also helped to protect against numerical artifacts that could otherwise obscure the proper physical conse-

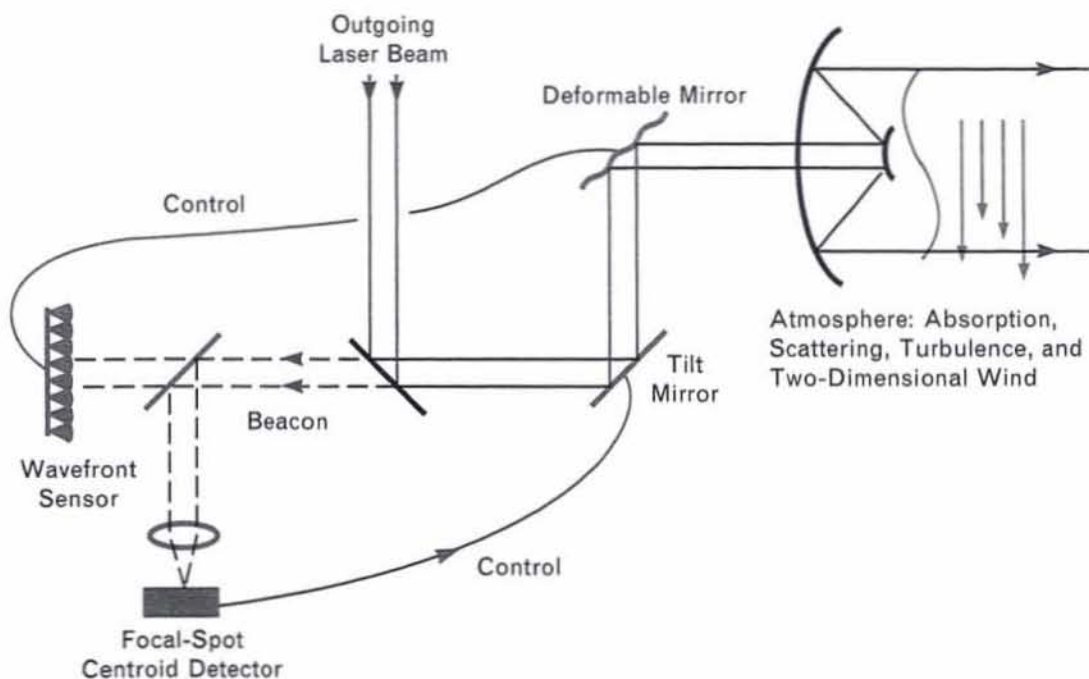


FIGURE 4. Model of compensated laser propagation in the MOLLY computer code.

quences of small-scale phenomena such as PCI and TTBI.

To conserve memory, we did not constrain the transverse grids on which MOLLY defines the high-power-laser field, beacon-laser field, and turbulent refractivity to the same size. (The grids for the laser-induced refractivity perturbations and the high-power laser are identical, however, as are the grids for the adaptive optics components and the beacon.) Even on the Cray-2 supercomputer, finite memory can significantly limit the simulation of thermal-blooming compensation, at least for very large laser systems. A typical MOLLY simulation defines laser-induced heating on 50 or so transverse grids with each grid having 300×300 or so points, and a more complex simulation can use as many as 400 grids of size 540×540 . For the simulation of propagation through the open air, such grids correspond to physical spacings as small as a few meters along the propagation direction, with a grid resolution of a few centimeters. Correspondingly, memory usage for a typical simulation is 20 Mwords or so, and the usage for a more complex simulation has been as large as 190 Mwords,

nearly 80% of the Cray-2's capacity.

MOLLY's software model of an adaptive optics system is shown schematically in Figure 4. As in a real system, adaptive compensation is shared between a flat mirror for tilt correction and a deformable mirror for higher-order correction. Each correction element is driven by its own sensor. The wavefront sensor can be either a Hartmann sensor [22], as indicated in the figure, or a shearing sensor [23]. MOLLY is also capable of modeling multidither compensation [24], which does not rely on a wavefront sensor *per se*. The deformable-mirror model includes such realities as broken actuators, finite response times, and limits on deformable-mirror stroke.

MOLLY uses a variety of atmospheric models. For simulation of the laboratory experiment described in Reference 15, MOLLY incorporates the precise absorptivity, refractivity, and placement of laboratory absorbing media. For simulations of field experiments in the real atmosphere, MOLLY can take atmospheric parameters as measured at discrete locations at the experimental site and, where necessary, interpolate to reconstruct a representation of the atmosphere in con-

tinuous space. For simulations of ballistic-missile-defense scenarios, MOLLY has used atmospheric parameters derived from measurements taken at the White Sands Missile Range in New Mexico by the Army Atmospheric Sciences Laboratory and supplemented by a model of random wind fluctuations (see the section "Simulation Results").

At the heart of the code, MOLLY represents a monochromatic, single-polarization optical beam by a complex scalar field ψ that advances along the propagation direction according to the paraxial equation

$$\left[2ikn \frac{\partial}{\partial z} + \nabla^2 + 2k^2 \delta n \right] \psi = 0, \quad (2)$$

where ∇^2 is the transverse Laplacian, k is the optical wave number, n is the ambient refractivity, and δn is the sum of turbulence- and laser-induced deviations from ambient refractivity. Strictly speaking, Equation 2 applies only to collimated laser propagation. Focused propagation (as occurs, for example, in the formation of a synthetic beacon) is reduced in MOLLY to Equation 2 by a coordinate transformation. The turbulence-induced refractivity perturbation, which the wind blows rigidly across the beam, is computed at initialization, before any numerical laser propagation takes place. The laser-induced contribution δn_L to δn is determined by

$$\left[\frac{\partial}{\partial t} + \mathbf{v} \cdot \nabla - \chi \nabla^2 \right] \delta n_L = -\frac{\alpha}{\rho c_p} \frac{dn}{dT} |\psi|^2, \quad (3)$$

where ψ is now the high-power-laser field, t is time, \mathbf{v} is wind (including the contribution of slew), and χ is the thermal diffusivity.

The paraxial equation is solved in MOLLY with the Fourier split-step algorithm [25]: propagation through a numerical range step of thickness Δz is divided into three substeps, as illustrated in Figure 5. In the first and third substeps (called phase half-steps), the paraxial equation is solved for step thickness $\Delta z/2$ by omitting the Laplacian term. In the second substep (called the vacuum step), the paraxial equation is solved for thickness Δz by omitting the refractivity term. This algorithm is computationally fast, amounting to simple point-by-point multiplication in the phase half-steps, and a fast Fourier trans-

formation and point-by-point multiplication in the vacuum step. The algorithm is also accurate—the error is $O(\Delta z^3)$ —and manifestly energy-conserving, so that it introduces no numerically spurious energy sources or sinks that could mask an amplification process such as PCI.

We also avoided spurious sources or sinks by calculating the wind transport and thermal diffusion (as defined by Equation 3) in the Fourier domain [25]: MOLLY advances the refractivity contribution δn_L through a time increment δt by adding δt times the right-hand side of Equation 3 to δn_L , Fourier-transforming the result, multiplying the Fourier transform by

$$e^{i\mathbf{p} \cdot \mathbf{v} \delta t - \chi p^2 \delta t}, \quad (4)$$

where \mathbf{p} is the Fourier wave vector and p is its magnitude, and inverse-Fourier-transforming the product. Smoothing at the grid boundaries is performed to avoid a numerical artifact known as Gibbs ringing [26]. In the absence of diffusion, this procedure is manifestly energy conserving because the multiplier given in Expression 4 has unit magnitude.

In interpreting MOLLY results, we must contend with two types of uncertainty: statistical and numerical. When turbulence is included, statistical uncertainty arises because random numbers are used in generating the turbulent refractivity patterns in the

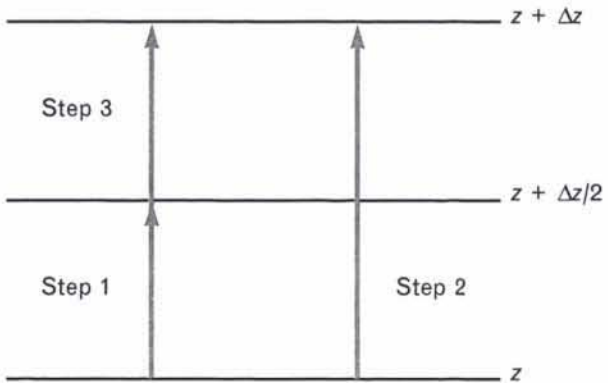


FIGURE 5. Schematic of the three substeps in one step of the Fourier split-step propagation algorithm. The propagation direction is up, and Δz is the thickness of one numerical step. The first and third substeps, each through distance $\Delta z/2$, ignore diffraction. The second substep, through the full thickness Δz , ignores refraction.

atmosphere. This kind of uncertainty is handled by simulating a propagation scenario several times, with different random numbers, to quantify the statistical spread. Numerical uncertainty arises because there is, at present, no practical theory of errors in the numerical modeling of thermal blooming. Numerical uncertainty is handled either (1) by simulating, when possible, a propagation scenario with various grid spacings and time steps, and verifying the insensitivity of the results to such numerical parameters, or (2) by identifying a trend that suggests a straightforward extrapolation to the continuum limit.

Simulation Results

We now present representative results drawn from simulations of a variety of laser systems. These results highlight the three questions that originally motivated the development of MOLLY, as well as of laboratory and field experiments conducted by Lincoln Laboratory. As stated previously, the questions are (1) is PCI real? (2) what physical processes ameliorate PCI? and (3) what is PCI's impact on the effectiveness of practical systems?

In a sense the first and second questions are closely intertwined. When PCI first became a pressing research concern, the standard practice in modeling and analyzing thermal blooming was to assume a uniform wind. This assumption, as we now know, tends to exaggerate PCI. In reality, natural wind in the open air is far from uniform. The variation of the wind with distance from the high-power-laser transmitter limits the strength of PCI that appears in scenarios of practical importance. For this reason, we have studied PCI in the limit of uniform wind and have investigated the amelioration of PCI by incorporating wind variation in the simulations.

One real contribution to the variation in natural wind is illustrated in Figure 6, which shows a natural spiral in the wind at Orogrande in the White Sands Missile Range [6], as measured in the lower atmosphere, where absorption is strongest. In addition to such an average spiral, the wind exhibits spatially random fluctuations with a strength of 5 to 15% of the mean, and with a characteristic length scale of up to $O(100)$ m. For ballistic-missile-de-

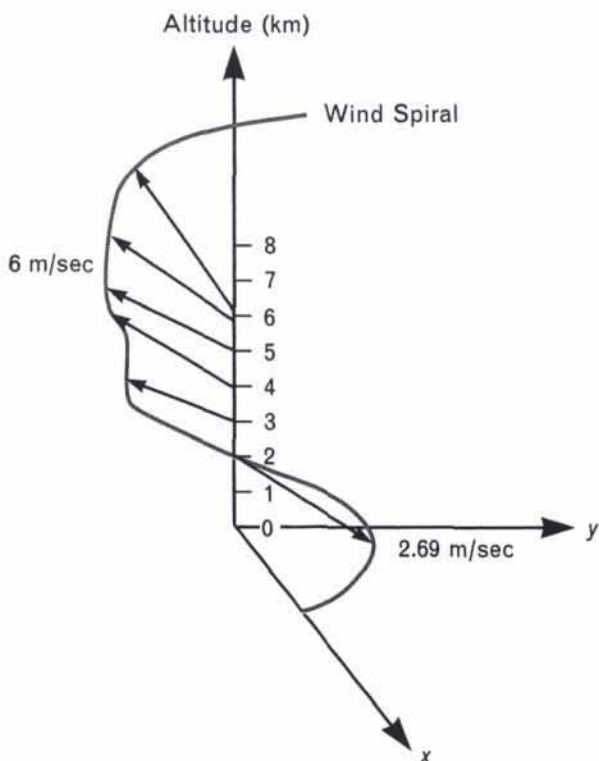


FIGURE 6. Wind spiral at Orogrande, White Sands Missile Range, N.M. [6].

fense scenarios in which the high-power beam is directed at a cooperative relay-mirror satellite, slew adds a nonuniform contribution of magnitude Ωz to the wind, where z is the distance from the transmitter and Ω is the slew rate (angle per time). For a relay mirror in low-earth orbit at altitude H directly overhead, Ω (in mrad/sec) is approximately $7.5/H$, for H in Mm. For a geosynchronous relay, Ω is essentially zero.

We use a number of diagnostics to identify PCI. Immediate visual evidence is provided by the dramatic growth of small-scale structures in the laser irradiance distribution, in the deformable-mirror figure, and in the phase of the corrected beam at the end of the absorbing medium, where the amplitude of phase variations should be minimal if adaptive compensation is successful. The latter diagnostic thus also serves as an indicator of exactly how PCI compromises adaptive optics performance. These indicators are most readily interpreted in the absence of turbulence, which produces irradiance scintillation even without PCI and which can corrupt the deformable-mirror figure and laser phase via TTBI.

We have obtained a more robust indicator of PCI by simulating the performance of a laser-propagation system under two different modes of operation. In the first mode, the adaptive optics loops are closed at the same time that transmission of the high-power laser beam is initiated, and performance is measured after one or a few wind-clearing times. This mode is referred to as the *ab initio* mode. In the second mode, called the *deferred* mode, the closing of the adaptive optics loops is delayed for a time after the beam is sent into the atmosphere, and performance is measured shortly after loop closure. The delay is typically one or a few wind-clearing times. Figure 7 illustrates these two modes. In the deferred mode, correction for thermal blooming should be relatively good. (There can be no PCI in this case because the adaptive optics system will have been on for too short a time for PCI to grow.) If, however, conditions are right for PCI to develop, then correction for thermal blooming will be relatively poor in the *ab initio* mode. This difference in thermal-blooming correction, which results from the opportunity for the adaptive optics feedback to generate PCI in the *ab initio* mode, has proven to be a useful signature for PCI. We now turn to specific results.

PCI Signatures for Uniform Wind

Figure 8 illustrates an extreme instance of PCI as diagnosed by the rapid growth of strong irradiance scintillation. Here, $N_D = 360$, the wind is uniform, and there are 340 adaptive optics actuators across the beam diameter for a corresponding very small $N_p \approx 0.013$. The figure shows the irradiance profile of the high-power beam at the end of the absorbing medium. Note that the beam evolves rapidly from smooth to highly scintillated in less than one third of a wind-clearing time. In Figure 9, the effects of strong PCI are evident in the highly uneven distribution of deformable-mirror actuator strokes in a simulation of a laboratory experiment [15] with $N_D = 240$ and 16 actuators across the beam for $N_p \approx 14$ (a value more typical of practical systems for transmission through long distances in the atmosphere). The effects of strong PCI are also evident in Figure 10 in the sizable and busy residual phase of the high-power laser beam as it exits the absorbing

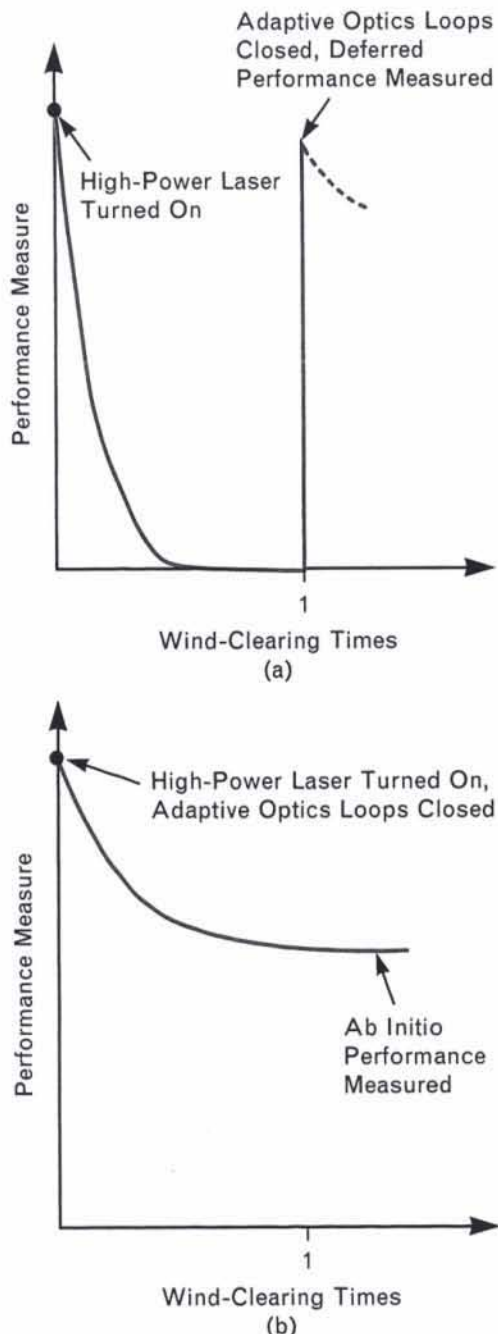


FIGURE 7. Illustration of (a) deferred and (b) *ab initio* behavior. Deferred behavior is measured after a high-power-laser beam has been on for a long time, but closure of the adaptive optics loops has been delayed until just before the measurement. *Ab initio* behavior is measured after a long transmission time during which the adaptive optics loops have been on from the start. Feedback between the adaptive optics hardware and the laser-induced heating affects the *ab initio* behavior but not the deferred behavior.

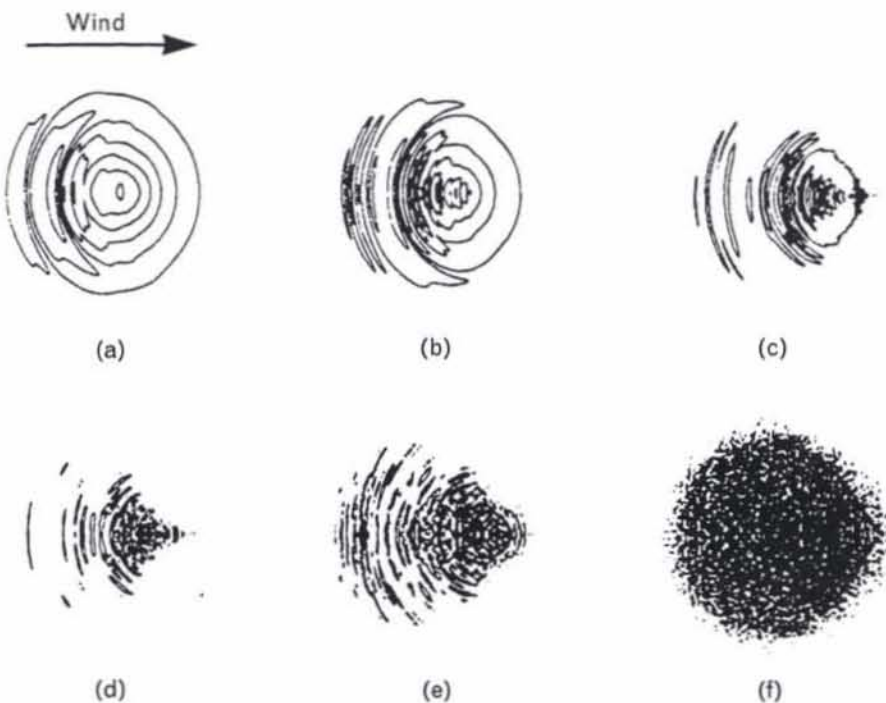


FIGURE 8. Contour plots of high-power-laser-beam irradiance at the end of the absorbing medium from a simulation with uniform wind, $N_D = 360$, $N_p = 0.013$, and time equal to (a) 0.2τ , (b) 0.225τ , (c) 0.25τ , (d) 0.275τ , (e) 0.3τ , and (f) 0.5τ , where τ is the wind-clearing time. The contour spacing is one-seventh the peak irradiance. These plots illustrate the rapid onset of PCI as seen in the development of a strong variation in laser irradiance on small spatial scales.

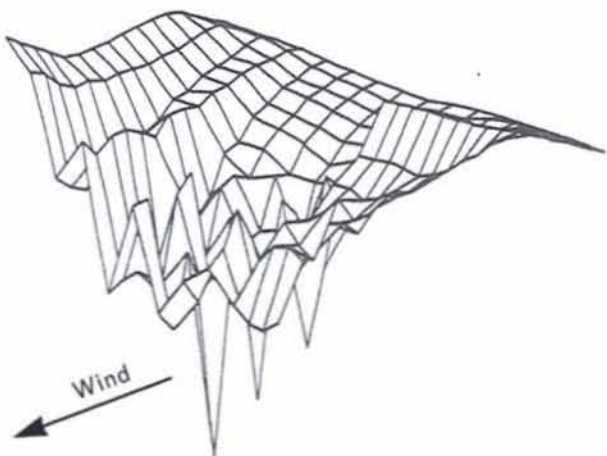


FIGURE 9. Deformable-mirror actuator positions, indicated by vertices in a stick figure, for a uniform-wind simulation of a thermal-blooming laboratory experiment [15] with $N_D = 240$ and 16 actuators across a beam diameter ($N_p = 14$). This illustration shows PCI as seen in the development of a strong variation in the adaptive optics phase correction on small spatial scales.

medium. The system is the same system as in Figure 9 but with a slightly larger $N_D = 270$.

The effects of strong PCI are evident in Figure 11, which shows the contrast between the ab initio and deferred peak far-field irradiances from uniform-wind simulations that included turbulence. In the simulations, there were 50 deformable-mirror actuators across the beam diameter for $N_p \approx 7$. As explained earlier, the ab initio results include feedback between the adaptive optics and the laser-induced heating, while the deferred results do not. Accordingly, the ab initio curve lies well below the deferred curve. Figure 12 provides a more direct illustration of the contrast between deferred and ab initio behavior for the system represented by Figure 11 by showing the residual phase of the high-power beam at the top of the atmosphere. As expected, the ab initio residual phase is much more corrupted than the deferred residual phase because of the feedback between the adaptive optics

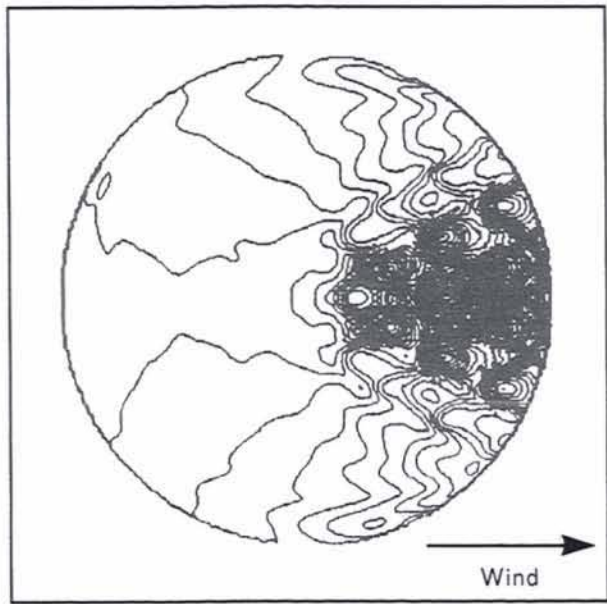


FIGURE 10. Phase of simulated high-power-laser beam at the end of the same distorting medium as in Figure 9, but with $N_D = 270$. The contour spacing is $\pi/2$ radians. This figure illustrates strong PCI as seen in the uncorrected portion of the outgoing high-power-laser phase.

system and laser-induced heating in the ab initio mode. Incidentally, the less severe but not insignificant corruption also seen in the deferred profile (Figure 12[b]) is an example of TTBI.

Perhaps the most striking indicator of PCI is the formation of organized patterns in the propagating optical fields. Figure 13(a) shows such a pattern that

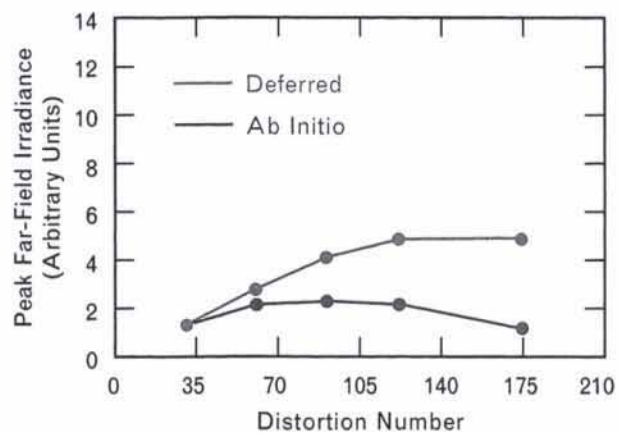


FIGURE 11. Peak far-field irradiance for ab initio and deferred compensation for combined thermal blooming and turbulence with a uniform wind and no slew. The actuator spacing is 1/50th the beam diameter for $N_p \approx 7$.

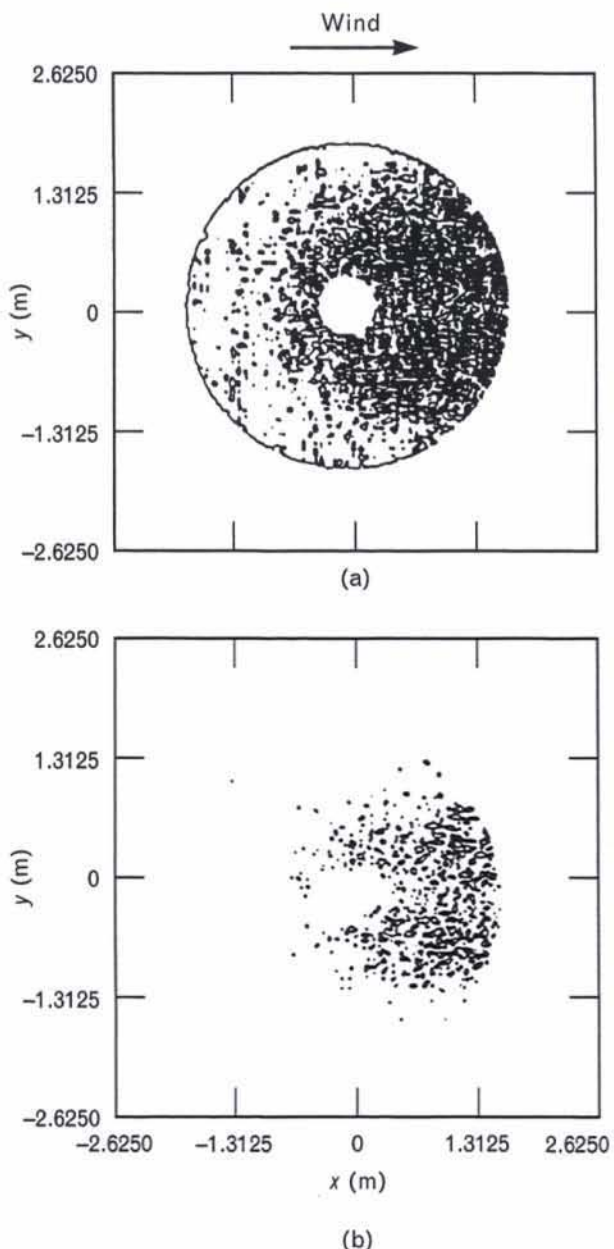


FIGURE 12. High-power-laser-beam phase at the end of the absorbing region after (a) ab initio and (b) deferred compensation for combined thermal blooming and turbulence with $N_D = 175$ and other parameters as in Figure 11. The contour spacing is 2π radians. These figures are the residual phases after attempted correction by the adaptive optics system. Because of feedback between the adaptive optics and the atmospheric heating, the residual phase is seen to be more significant in the ab initio than in the deferred case. The less severe residual phase in the deferred picture is a consequence of turbulence/thermal-blooming interaction (TTBI).

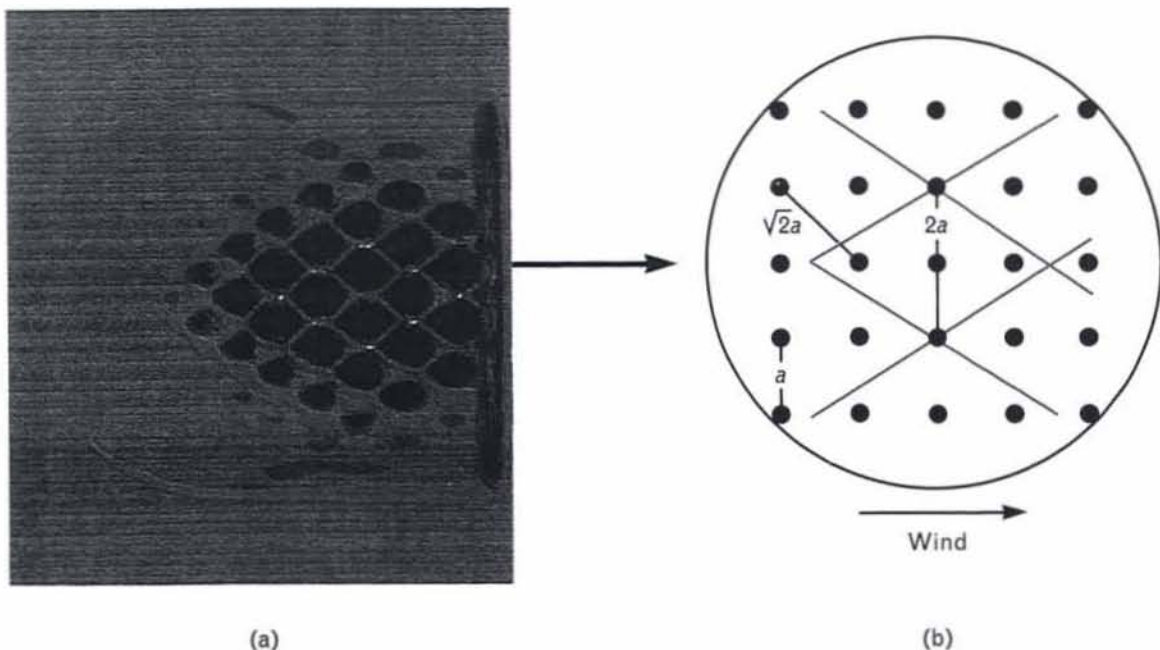


FIGURE 13. An important quantitative signature of PCI: (a) Pattern formation in the irradiance distribution of a beacon beam entering an adaptive optics system. The pattern was obtained from simulation of a thermal-blooming laboratory experiment [15] with uniform wind, $N_D = 300$, and 16 actuator spacings across the beam ($N_p \approx 14$). (b) Diagram calibrates the pattern's unit cell (blown up) in terms of a , the deformable-mirror actuator spacing.

formed spontaneously in the irradiance distribution of a beacon beam as it entered an adaptive optics system. We obtained this dramatic signature of strong PCI in a computer simulation of the thermal-blooming laboratory experiment [15] with $N_D = 300$, 16 actuators across the beam, and $N_p \approx 14$. Although the simulation is idealized in the sense that it does not include imperfections such as defective actuators (which are present in the real experiment), similar patterns have in fact been seen in the laboratory [15]. In the figure, a chainlink pattern is evident. The diagram in Figure 13(b) indicates that the diamond-shaped unit cell of the chainlink pattern is two actuator spacings wide across the wind and three actuator spacings long along the wind.

The diamond shape and the aspect ratio 3:2 have both been successfully predicted by a linearized analysis [20]. The main output of the linearized theory of PCI is a set of growth rates for perturbations in laser fields or in atmospheric heating (see the box, "Linear-

ized Analysis of Phase-Compensation Instability"). The theory produces a variety of such growth rates that correspond to characteristic PCI modes, which are analogous to the characteristic modes of vibration of, for example, a drumhead. The pattern that stands out in a picture such as Figure 13 is dominated by modes whose growth rates have the largest real part. For the scenario in Figure 13, it can be shown [20] that there are four such dominant modes, whose superposition is in close correspondence with the observed chainlink pattern (discussed in the box, "Linearized Analysis of Phase-Compensation Instability"). This correspondence is especially impressive because, strictly speaking, the thermal blooming in Figure 13 is actually too strong for the application of linearized analysis.

Processes That Ameliorate PCI

Figure 14 illustrates how PCI is ameliorated by incorporating wind variation into the simulation. The

scenario is the same as in Figures 11 and 12, except the uniform wind is now supplemented by a slew that causes an approximate quadrupling of the total wind speed between the high-power-laser transmitter and the end of the absorbing medium. Figure 14 shows curves of deferred and ab initio peak far-field irradiances, just as does Figure 11. Note that although the ab initio curve lies well below the deferred curve in Figure 11, the two curves in Figure 14 are very close, indicating that the slew-induced variability in wind has suppressed the growth of PCI.

In principle, we can eliminate PCI by using *full-field-conjugate*, rather than phase-conjugate, adaptive optics to compensate for thermal blooming [14]. With full-field conjugation, the beacon and the outgoing laser have the same wavelength, the outgoing phase is conjugate to the incoming phase, and the outgoing irradiance pattern must be equal to the incoming pattern, up to an overall gain multiplier. In phase-conjugate adaptive optics, on the other hand, the outgoing irradiance is unrelated to the incoming irradiance and the outgoing and incoming wavelengths need not be equal.

The potential of full-field conjugation is illustrated in Figure 15, which shows irradiance profiles of

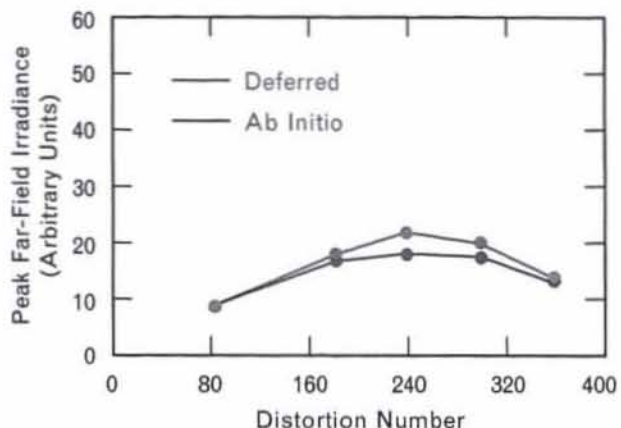


FIGURE 14. Peak far-field irradiance for ab initio and deferred compensation for combined thermal blooming and turbulence. The data are for uniform natural wind plus slew that roughly quadruples the total wind speed between the high-power-laser transmitter and the top of the absorbing medium. The atmospheric, adaptive optics, and beam parameters are as in Figure 11.

two high-power-laser beams at the end of a common uniform-wind absorbing medium after one wind-clearing time of propagation with $N_D = 330$. In Figure 15(a), thermal blooming is compensated by a phase-conjugate adaptive optics system with a very fine actuator spacing, as in Figure 8. In Figure 15(b), thermal blooming is compensated by full-

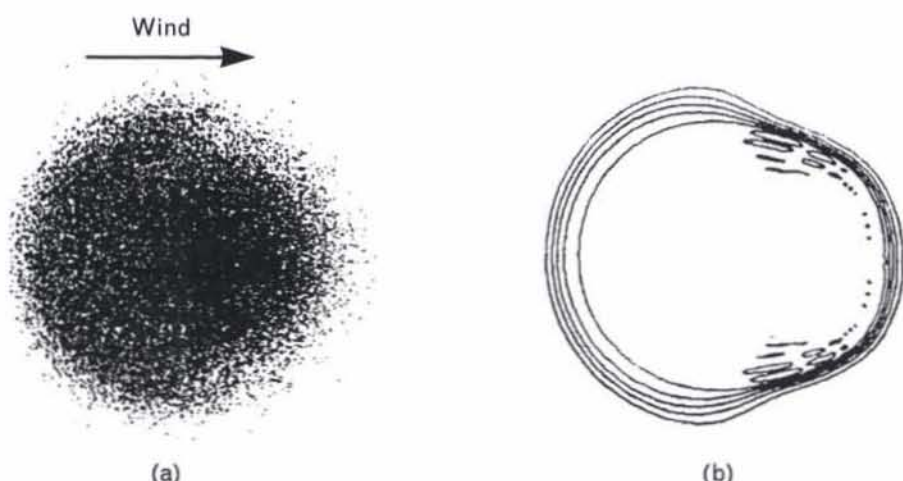


FIGURE 15. Contour plots of high-power-laser-beam irradiance at the end of the absorbing medium after one wind-clearing time, from uniform-wind simulations with (a) very-high-resolution phase-conjugate adaptive optics ($N_p = 0.013$) and (b) full-field-conjugate adaptive optics. The value of N_D is 330, and the contour spacing is one-seventh the peak irradiance. The plots illustrate the potential of full-field-conjugate adaptive optics for suppressing PCI.

LINEARIZED ANALYSIS OF PHASE-COMPENSATION INSTABILITY

THE EQUATIONS that govern the detailed dynamics of thermal blooming (Equations 2 and 3 in the main text) turn out to be easy to solve in closed form when the laser fields and refractivity are assumed to be uniform in space. Thus it is common to analyze the dynamical equations of thermal blooming by expanding all equations to linear order about the uniform solution. References 1 and 2 specify the resulting linear system in detail.

The linearized equations of thermal blooming take the general form

$$\frac{d(\delta n_L)}{dt} = H(\delta n_L),$$

where δn_L is the laser-induced contribution to refractivity, t is time, and H is a linear operator that depends on the wind, absorptivity, and other atmospheric properties, and also on the details of the adaptive optics compensation. In phase-conjugate compensation, the operator H has an eigenvalue spectrum so that, in general, any δn_L is a sum of eigenmodes, each evolving in time as

$\exp(\omega t)$, where ω is the corresponding eigenvalue, or growth rate, of phase-compensation instability (PCI). In view of the exponential character of this time development, the mode(s) with the eigenvalue(s) with the largest real part will dominate the appearance of propagating fields for very large t .

The linearized equations of thermal blooming simplify considerably when they have been Fourier transformed with respect to the directions transverse to the direction of propagation [1, 2]. One finds that a general PCI eigenmode, characterized by a two-component vector p , is a sum of Fourier components with wave vectors of the general form $p + 2\pi n/a$, where n is a two-component vector with both components integers and a is the actuator spacing of the deformable mirror [2]. As a practical matter, the dominant PCI growth rate can be obtained by first calculating the real part of the dominant growth rate for fixed p —which is a doubly periodic function of p with periods $(0, 2\pi/a)$ and

$(2\pi/a, 0)$ —and then searching for the global maximum.

Figure A shows a contour plot that we computed [2] for the real part of the p -dependent dominant growth rate for the simulation scenario of Figure 13 in the main text. The axes do not extend beyond $\pm\pi/a$ in any direction because of double periodicity. The dominant modes correspond to the peaks in Figure A, which occur at wave vector $(\pm 2\pi/3a, \pm\pi/a)$, where the x axis lies along the wind. These modes, which correspond in real space to ripples with period $2a$ in y and $3a$ in x , are in good agreement with the crisscrossing lines that make up the chainlink pattern in Figure 13 in the main text.

References

1. T.J. Karr, "Thermal Blooming Compensation Instabilities," *J. Opt. Soc. Am. A* 6, 1038 (1989).
2. J.F. Schonfeld, "Linearized Theory of Thermal-Blooming Phase-Compensation Instability with Realistic Adaptive Optics Geometry," to be published in *J. Opt. Soc. Am. B*; J.F. Schonfeld and B. Johnson, "Pattern Formation from Thermal Blooming Phase-Compensation Instability," to be published in *J. Opt. Soc. Am. B*.

field conjugation. Note that in the phase-conjugate case the beam is highly scintillated, while in the full-field-conjugate case hardly any scintillation can be seen. Ideally, full-field conjugation would be accomplished with passive nonlinear-optical materials, rather than by the electro-optical-mechani-

cal hardware used in conventional phase-conjugate adaptive optics. (Reference 27 discusses the limitations to PCI suppression in real nonlinear-optical media.) Full-field-conjugate correction for strong thermal blooming has yet to be demonstrated experimentally.

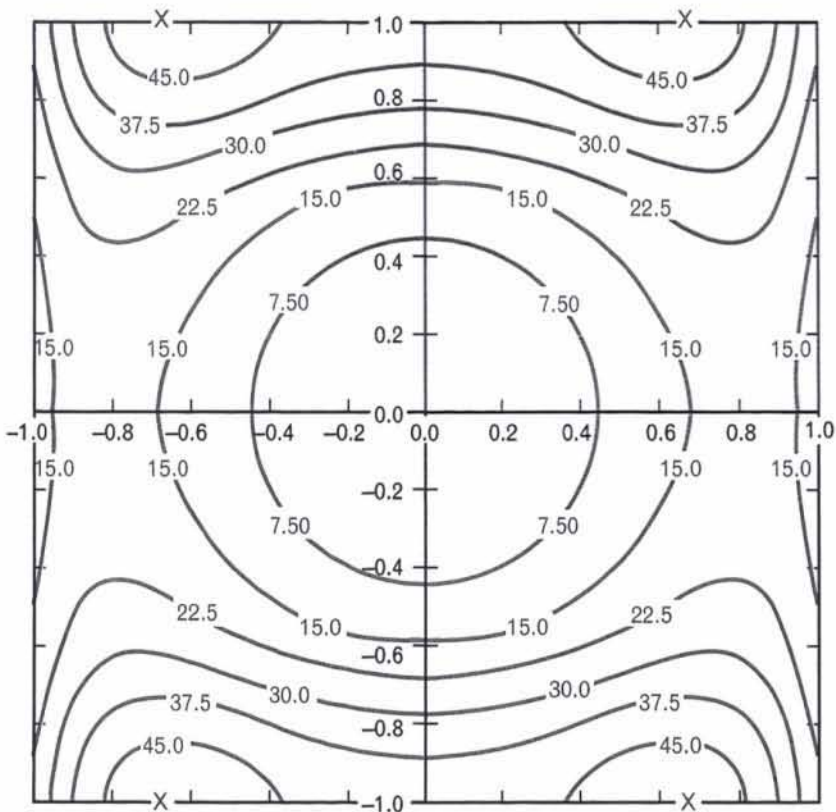


FIGURE A. Contour plot of the real part of the dominant PCI growth rate (in Hz) as a function of the spatial wave vector for the scenario of Figure 13 in the main text. The maxima are indicated by red Xs and the coordinate axes are calibrated in units of π/a , where a is the actuator spacing of the deformable mirror.

Practical Systems

Our most realistic simulations of prospective practical systems have been done in the context of a study on *scaling*. Scaling is of particular importance in an area such as ballistic-missile defense, in which the full-scale system that would ultimately be built is considerably larger, more powerful, and more expensive than the exploratory or proof-of-principle systems used to gain the confidence necessary to undertake full-scale deployment. The object of a scaling study is to identify credible trends, if they exist, that might enable the easy extrapolation from the results of a subscale experiment to the performance of a full-scale system. A number of researchers have attempted to derive such scaling

trends from theoretical arguments, but to date no clear consensus has emerged. We have attempted to resolve the matter empirically with MOLLY simulations.

Figure 16 shows the results of such an exercise for vertical, zero-slew propagation at $1.06 \mu\text{m}$ from ground to space at the White Sands Missile Range. An adaptive optics system with an actuator spacing of 7.5 cm corrected the propagation. The figure shows quite clearly that a simple scaling trend exists. Strehl ratio—the ratio of the actual peak far-field irradiance to the peak far-field irradiance in the diffraction limit—depends on laser power P and diameter D only through the combination $P/D^{1.5}$; i.e., a big system and a small system with a common wavelength and actuator spacing will exhibit roughly the same Strehl ratio as long

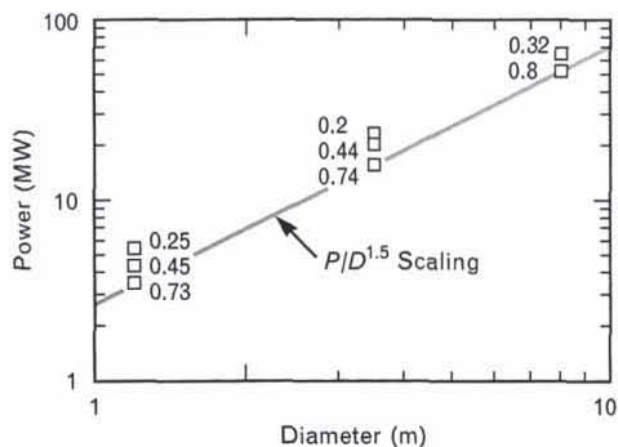


FIGURE 16. Strehl ratios for various power/diameter pairs from simulations of compensated vertical 1.06- μm propagation at White Sands Missile Range with an adaptive optics actuator spacing of 7.5 cm ($N_p = 8$). For reference, N_D is 182 for simulation with power 15.9 MW and diameter 3.5 m. The line connects points with a common value of power/diameter $^{1.5}$.

as they share a common value of $P/D^{1.5}$. Note that the simulations represented in Figure 16 omit spatially random fluctuations around the nonuniform mean wind. Because of limitations in time and funding, we were unable to repeat all of the simulations with the random fluctuations included. Nevertheless, an incomplete set of results with fluctuations suggests that if two systems share a common value of $P/D^{1.5}$, the larger-diameter system will exhibit the higher Strehl ratio. These results should be valuable for future designers of large, high-power-laser propagation systems.

Even though we found the Strehl ratios to be high for the largest systems in Figure 16, these systems in fact also exhibited pattern formation indicative of

PCI. Thus significant PCI can coexist with good system performance. This result—that the Strehl ratio can remain high in spite of the onset of PCI—is encouraging because it shows that PCI does not pose the threat to practical large-system performance that had once been feared.

Summary

We have surveyed more than 20 years of thermal-blooming theory at Lincoln Laboratory with an emphasis on work performed since 1985, most prominently the development of the computer-code MOLLY. With MOLLY, we have been able to address the three basic questions that motivated the code's development in the first place. Results from MOLLY have confirmed (1) that PCI is a real physical phenomenon that behaves in quantitative accord with analytical predictions, (2) that PCI is ameliorated by slew and the realistic variation of natural wind, and (3) that PCI can coexist with good correction for thermal blooming. In addition, results from MOLLY have demonstrated trends that have facilitated the prediction of the performance of large thermal-blooming-compensation systems from subscale experiments.

Acknowledgments

MOLLY was developed with the assistance of three talented and dedicated programmers: Gregory S. Rowe, Stephen K. Grasberger, and Michael E. O'Brien. The Strategic Defense Initiative Organization and the Army Strategic Defense Command through the Air Force sponsored MOLLY's development and application, as well as the related analytical work.

REFERENCES

1. D.P. Greenwood and C.A. Primmerman, "Adaptive Optics Research at Lincoln Laboratory," in this issue.
2. J.W. Hardy, "Active Optics: A New Technology for the Control of Light," *Proc. IEEE* **66**, 651 (1978).
3. P.B. Ulrich and L.E. Wilson, eds., "Propagation of High-Energy Laser Beams through the Earth's Atmosphere," *Proc. SPIE* **1221** (1990). (Note: This reference provides a snapshot of the field as of early 1990. Important work not represented in the aforementioned volume has also been done by members of the JASON group, most notably M.N. Rosenbluth, P.H. Diamond, and F.W. Perkins.)
4. F.X. Kneizys, E.P. Shettle, L.W. Abreu, J.H. Chetwynd, G.P. Anderson, W.O. Gallery, J.E.A. Selby, and S.A. Clough, "User's Guide to LOWTRAN 7," *Air Force Geophysics Laboratory Report AFGL-TR-88-0177* (16 Aug. 1988).
5. S. Fulghum and M. Tilleman, "Interferometric Calorimeter for the Measurement of Water Vapor Absorption," to be published in *J. Opt. Soc. Am. B* (Dec. 1991).
6. "A Model of the Atmosphere from 0–30 km at the White Sands Missile Range," *U.S. Army Ground-Based-Laser Project Office (White Sands Missile Range, NM) Report K6DM-12188* (31 Jan. 1989).
7. L.C. Bradley and J. Herrmann, "Phase Compensation for Thermal Blooming," *Appl. Opt.* **13**, 331 (1974).
8. J. Herrmann, private communication.
9. J. Herrmann, "Properties of Phase Conjugate Adaptive Optical Systems," *J. Opt. Soc. Am.* **67**, 290 (1977).
10. J. Herrmann, private communication.
11. Linearized analysis of PCI was foreshadowed in the unpublished work of H.C. Pradadaude of Lincoln Laboratory in 1986.
12. R.B. Myers, North East Research Associates (Woburn, MA), unpublished.
13. R.J. Briggs, "Models of High-Spatial-Frequency Thermal Blooming Instabilities," *Lawrence Livermore National Laboratory Report UCID-21118* (14 Aug. 1987).
14. T.J. Karr, "Thermal Blooming Compensation Instabilities," *J. Opt. Soc. Am. A* **6**, 1038 (1989).
15. B. Johnson, "Thermal-Blooming Laboratory Experiments," in this issue.
16. L.C. Bradley and J. Herrmann, "Numerical Calculation of Light Propagation in a Nonlinear Medium," *J. Opt. Soc. Am.* **61**, 668 (1971), paper TuG11.
17. J.F. Schonfeld, "Analysis and Modeling of Thermal-Blooming Compensation," *Proc. SPIE* **1221**, 118 (1990).
18. The name was suggested by Marvin Litvak.
19. Private communication.
20. J.F. Schonfeld, "Linearized Theory of Thermal-Blooming Phase-Compensation Instability with Realistic Adaptive Optics Geometry," to be published in *J. Opt. Soc. Am. B*; J.F. Schonfeld and B. Johnson, "Pattern Formation from Thermal Blooming Phase-Compensation Instability," to be published in *J. Opt. Soc. Am. B*.
21. R.A. Humphreys, L.C. Bradley, and J. Herrmann, "Sodium-Layer Synthetic Beacons for Adaptive Optics," in this issue.
22. H.T. Barclay, P.H. Malyak, W.H. McGonagle, R.K. Reich, G.S. Rowe, and J.C. Twichell, "The SWAT Wavefront Sensor," in this issue.
23. C.L. Koliopoulos, "Radial Grating Lateral Shear Heterodyne Interferometer," *Appl. Opt.* **19**, 1523 (1980).
24. T.R. O'Meara, "The Multidither Principle in Adaptive Optics," *J. Opt. Soc. Am.* **67**, 306 (1977).
25. J.A. Fleck, Jr., J.R. Morris, and M.D. Feit, "Time-Dependent Propagation of High Energy Laser Beams through the Atmosphere," *Appl. Phys.* **10**, 129 (1976).
26. C. Canuto, M.Y. Hussaini, A. Quarteroni, and T.A. Zang, *Spectral Methods in Fluid Dynamics* (Springer-Verlag, New York, 1988).
27. J.F. Schonfeld, "Instability in Saturated Full-Field Compensation for Thermal Blooming," to be published in *J. Opt. Soc. Am. B*.



JONATHAN F. SCHONFELD was raised in New Rochelle, New York, and received a B.S. degree, summa cum laude, in mathematics and physics from Yale University in 1972, and a Ph.D. in physics from Princeton University in 1975 as a National Science Foundation Predoctoral Fellow. He worked on the theory of elementary particles at the California Institute of Technology, the University of Minnesota, the Ecole Normale Supérieure in Paris, and the Fermi National Accelerator Center (Fermilab) before joining Lincoln Laboratory in 1985. In elementary-particle physics, he is best known for his contributions to the theory of planar quantum fields, and to the statistical mechanics of colliding beams in electron-positron storage rings. As a member of the High-Energy-Laser Beam Control and Propagation Group at Lincoln Laboratory, he specialized until recently in the theory of adaptive optics, principally as applied to thermal-blooming compensation. He is currently a member of the Advanced Techniques Group, where he has been working on advanced signal-processing problems.